REPORT DOCUMENTATION PAGE

Form Approved
OMB No. 0704-0188

1. REPORT DATE *(DD-MM-YYYY)*	2. REPORT TYPE	3. DATES COVERED *(From - To)*
06-08-2009	Journal Article	

4. TITLE AND SUBTITLE
An Automated De-striping Algorithm for Ocean Color Monitor Imagery

5a. CONTRACT NUMBER

5b. GRANT NUMBER

5c. PROGRAM ELEMENT NUMBER
N/A

6. AUTHOR(S)
Paul Lyon

5d. PROJECT NUMBER

5e. TASK NUMBER

5f. WORK UNIT NUMBER
73-8669-06-5

7. PERFORMING ORGANIZATION NAME(S) AND ADDRESS(ES)
Naval Research Laboratory
Oceanography Division
Stennis Space Center, MS 39529-5004

8. PERFORMING ORGANIZATION REPORT NUMBER
NRL/JA/7330-07-7209

9. SPONSORING/MONITORING AGENCY NAME(S) AND ADDRESS(ES)
Office of Naval Research
800 N. Quincy St.
Arlington, VA 22217-5660

10. SPONSOR/MONITOR'S ACRONYM(S)
ONR

11. SPONSOR/MONITOR'S REPORT NUMBER(S)

12. DISTRIBUTION/AVAILABILITY STATEMENT
Approved for public release, distribution is unlimit

13. SUPPLEMENTARY NOTES

14. ABSTRACT
Ocean Colour Monitor, OCM, is a push broom sensor design with 3740 detectors across scan for each of its eight channels. Along track striping caused by poorly characterised detector to detector calibration results in derived ocean colour products that are hardly usable. Because OCM is turned on only for purposed orbits, the coefficients needed to correct each cross scan detector are not constant for all orbits. An algorithm has been developed to remove the effects of striping which is based on the information contained in each image. The algorithm performance depends only on the quantity of contiguous pixels over the water for each detector. Along scan detectors that have sufficient water pixels within the image to derive statistically significant correction coefficients are corrected with a fixed vector of scale factors. This paper outlines the automated de-striping algorithm (ADM), shows the results of ADM, quantifies the improvement to the images achieved and describes the limitations of the method.

15. SUBJECT TERMS
OCM, algorithm, detectors, ADM

16. SECURITY CLASSIFICATION OF:			17. LIMITATION OF ABSTRACT	18. NUMBER OF PAGES	19a. NAME OF RESPONSIBLE PERSON
a. REPORT	b. ABSTRACT	c. THIS PAGE			Paul Lyon
Unclassified	Unclassified	Unclassified	UL	10	19b. TELEPHONE NUMBER *(Include area code)* 228-688-4971

International Journal of Remote Sensing
Vol. 30, No. 6, 20 March 2009, 1493–1502

Taylor & Francis
Taylor & Francis Group

An automated de-striping algorithm for Ocean Colour Monitor imagery

P. E. LYON*
Ocean Optics Section, Oceanography Division, Naval Research Laboratory

(*Received 31 July 2007; in final form 17 December 2007*)

Ocean Colour Monitor, OCM, is a push broom sensor design with 3740 detectors across scan for each of its eight channels. Along track striping caused by poorly characterised detector to detector calibration results in derived ocean colour products that are hardly usable. Because OCM is turned on only for purchased orbits, the coefficients needed to correct each cross scan detector are not constant for all orbits. An algorithm has been developed to remove the effects of striping which is based on the information contained in each image. The algorithm performance depends only on the quantity of contiguous pixels over the water for each detector. Along scan detectors that have sufficient water pixels within the image to derive statistically significant correction coefficients are corrected with a fixed vector of scale factors. This paper outlines the automated de-striping algorithm (ADM), shows the results of ADM, quantifies the improvement to the images achieved and describes the limitations of the method.

1. Introduction

Space borne sensors can provide global coverage of ocean features, in-water optical properties and concentrations of phytoplankton, dissolved organic matter and suspended sediments. There are many satellites now on orbit that in-water optical properties can be derived from. The ocean colour monitor (OCM) is a 360 m resolution, push-broom sensor with 3740 detectors across scan for each of its eight spectral channels. Table 1 lists the spectral distribution of these channels. The spectral channels used on this sensor are the same channels used on the SeaWiFS sensor. Therefore, atmospheric correction and optical property algorithms designed to work with SeaWiFS data can be used on OCM data. The National Aeronautics and Space Administration (NASA) has developed a suite of computer programs for satellite data processing called SeaDAS. The software tool suite is designed to process ocean colour data from multiple satellite sensors including SeaWiFS, MODIS, OCTS, and CZCS. SeaDAS is developed and freely distributed by the SeaDAS Development Group at NASA Goddard Space Flight Center. The program in the SeaDAS tool suite that is used to convert top of atmosphere radiance to in-water products is called MSl12. The Naval Research Laboratory (NRL) has added OCM data processing capability to NRL's version of MSl12 which all images shown in this paper have been processed with.

OCM flies on IRS-P4 in a polar, sun synchronous orbit with 98.28° inclination at an altitude of 720 km. The data are not stored onboard, but are broadcast on X-band transmissions to ground stations. OCM data are purchased on a per orbit

*Email: paul.lyon@nrlscc.navy.mil

International Journal of Remote Sensing
ISSN 0143-1161 print/ISSN 1366-5901 online
http://www.tandf.co.uk/journals
DOI: 10.1080/01431160802468263

Table 1. The bands of both SeaWiFS and OCM are listed, showing that the bands available on OCM are nearly identical to SeaWiFS. The atmospheric correction and optical property algorithms designed for SeaWiFS can be directly applied to OCM data.

	SeaWiFS	OCM
Band	Wavelength (nm)	Wavelength (nm)
1	402–422	404–423
2	433–453	431–451
3	480–500	475–495
4	500–520	501–520
5	545–565	547–565
6	660–680	660–677
7	745–785	749–787
8	845–885	847–882

basis. The satellite is only turned on for orbits which have been purchased. The state of the system for any one pass depends on whether the previous orbit was purchased or not. Therefore a single characterization of the detector array cannot be derived from one image or a subset of images, and applied to all other images to correct the striping.

Figure 1 is a false colour image of top of atmosphere radiance at 412 nm, L_T (412 nm) which shows the typical level of striping found in an image from OCM. Each spectral channel has a different level of striping, and is not correlated with the striping in other channels. The striping noise from all the channels used to atmospherically correct the image, or to derive the in-water properties, affects the in-water optical products. Figure 2 is an example of detrital and dissolved organic matter absorption at 412 nm, a_{dg} (412 nm), derived from the quasi-analytical algorithm (QAA) applied to striped OCM data (Lee *et al* 2002). The level of striping in the derived product makes visual inspection of the in-water features difficult, and causes large errors in the pixel-to-pixel estimates of the derived products.

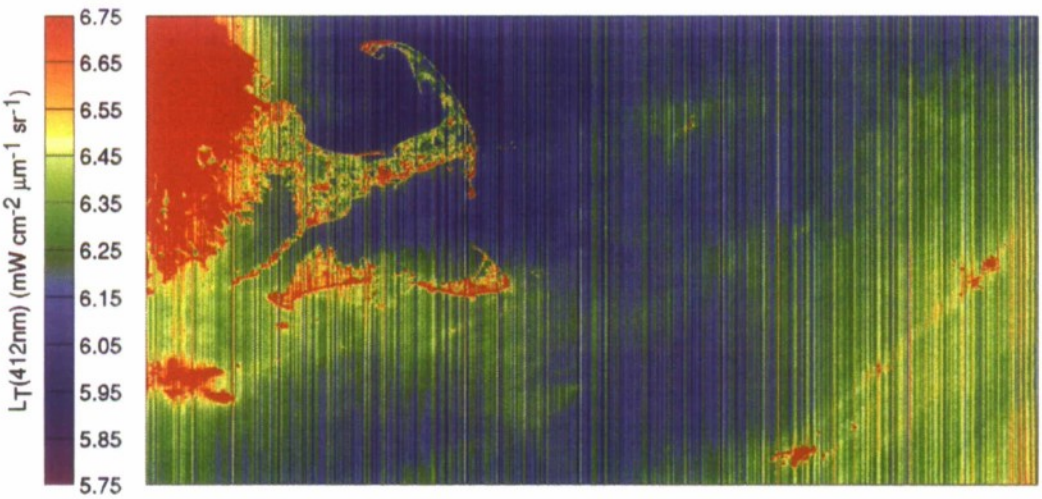

Figure 1. A false colour image of a subsection of top of atmosphere radiance, L_T(412 nm), measured by OCM which is an example of the typical level of striping found in OCM data. The land masses on the left portion of the image are Cape Cod, Martha's Vineyard Island and Nantucket Island Massachusetts.

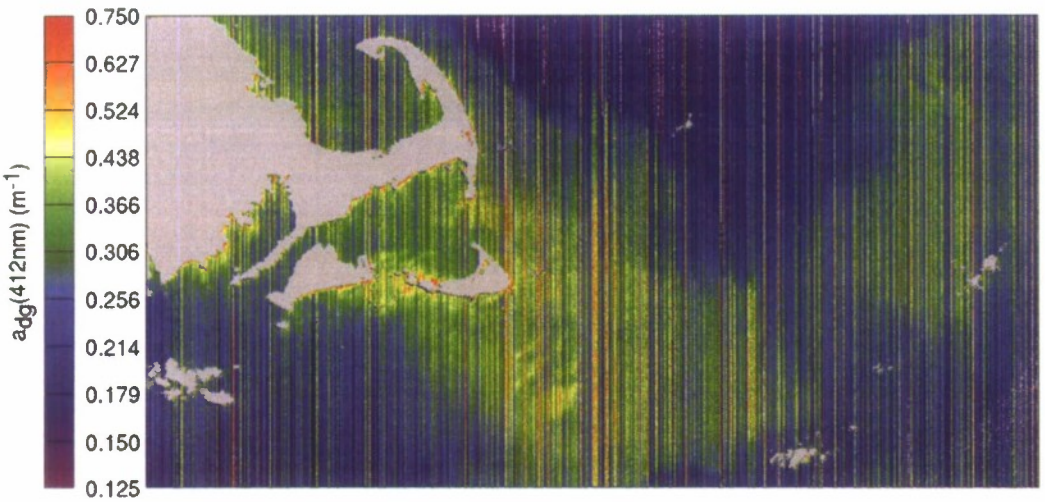

Figure 2. A false colour image of a derived optical product, coloured dissolved organic matter absorption coefficient at 412 nm, a_{dg}(412 nm) showing the level of striping depicted is typical for products derived from multiple OCM bands. Each OCM band has a different level of striping and the striping is not correlated from one band to another. Note that some in-water features can be discerned from the image. However, the level of striping makes a detailed analysis difficult if not impossible to complete.

As the state of the OCM electronics varies from orbit to orbit, an automatic de-striping algorithm (ADM) is needed that depends only on information that can be attained from the image data. There are many published techniques that are used to remove striping from images such as the histogram matching (Horn and Woodham 1979, Poros and Peterson 1985, Wegener 1990), moment matching (Ahern *et al.* 1984, Fischel 1984, Csillag and Smith 2000, Gadallah *et al.* 2000) and Fourier transform filter methods (Simpson *et al.* 1998, Chen *et al.* 2003, Chen *et al.* 2006). Many of the published de-striping methods are developed for horizontal striping caused by a small number of detectors that are swept across the image producing a periodic signal with a period determined by the number of along track detectors per channel. As stated above, OCM is a push broom sensor so there is no periodicity associated with the striping. The technique described here differs from these other techniques in that it doesn't rely on any periodic variation in the striping. It takes advantage of the fact that in-water features tend to smoothly vary spatially over scales of tens of kilometers while the noise induced by the poorly characterised detectors varies at the spatial resolution of the sensor. In the case of OCM, the spatial resolution variability is on the order of 300 m. There are two other published techniques that are similar to the ADM described here, Corsini *et al.* 2000, and Crippen 1989. The Corsini *et al.* de-striping algorithm derived for MOS-B data relied on carefully selected homogeneous targets from multiple images, and assumed that once derived, the correction coefficients (in their solution gains and offsets) could be applied to all images detected by the MOS-B sensor. The Crippen method was derived for Landsat Thematic Mapper land imagery and is mathematically similar to the method describe here. However, the Crippen method derives a correction coefficient for each pixel which is subtracted from the pixel. The Crippen method therefore derives a matrix of correction coefficients, not a detector to detector characterization vector derived by the ADM described here.

2. Methods

The voltage measured on each detector is proportional to the number of photons collected by the detector during the integration time. The voltage measured at each detector is converted to a digital number (DN) by an analogue to digital converter. The DN for the ith detector is converted to top of atmosphere radiance for the jth image pixel and wavelength λ, $L_T(\lambda)_{i,j}$

$$L_T(\lambda)_{i,j} = (\mathrm{DN})(\lambda)_{i,j} s(\lambda)_i + b(\lambda)_i \tag{1}$$

where $s(\lambda)_i$ and $b(\lambda)_i$ are the calibration scale and bias for the ith detector determined pre-flight. As the pre-flight scale and bias values are not available to convert $L_T(\lambda)_{i,j}$ back to DN, the ADM described here derives de-striping coefficients that are applied directly to $L_T(\lambda)_{i,j}$. Therefore the de-striped top of atmosphere radiance $L_{DT}(\lambda)_{i,j}$ is derived from

$$L_{DT}(\lambda)_{i,j} = L_T(\lambda)_{i,j} K(\lambda)_i + B(\lambda)_i \tag{2}$$

and

$$L_{DT}(\lambda)_{i,j} = (\mathrm{DN})(\lambda)_{i,j} s(\lambda)_i K(\lambda)_i + K(\lambda)_i b(\lambda)_i + B(\lambda)_i \tag{3}$$

where $K(\lambda)_i$ and $B(\lambda)_i$ are the ADM derived scale and bias. As shown in equation (3), the ADM-derived scale affects the pre-flight determined calibration scale and bias. Analysis of OCM imagery and variation of the ADM showed that $B(\lambda)_i$ is typically much less than 5% of $L_T(\lambda)$. If $B(\lambda)_i$ is small enough to ignore, the de-striped top of atmosphere radiance can be derived from

$$L_{DT}(\lambda)_{i,j} = (\mathrm{DN})(\lambda)_{i,j} s(\lambda)_i K(\lambda)_i + K(\lambda)_i b(\lambda)_i \tag{4}$$

A version of the ADM that derived both $K(\lambda)_i$ and $B(\lambda)_i$ was compared with one that derived only $K(\lambda)_i$ and it was found that there was no benefit to using equation (3) instead of equation (4) in the ADM, therefore the ADM describe herein is based on equation (4). This choice simplifies the implementation of the ADM by replacing the linear regression to derive both $K(\lambda)_i$ and $B(\lambda)_i$ with a computationally faster derivation of $K(\lambda)_i$ described below.

An image acquired by one ground station is typically 12 000 lines long. Each image is divided up into sections called chunks. The number of lines used in each chunk is configurable in the software implementation of the ADM. For the spatial resolution of OCM, it was found that 100 line chunks work well. The number of chunks obviously depends on the number of lines in each image and the number of lines in each chunk. Within each chunk, the indices of all pixels that are over water for each ith detector are stored in vector $\mathbf{p}$. The magnitude of the L_T(865 nm) band is used to identify and mask land, cloud and glint pixels. For each ith detector, N_i represents the number of water pixels that are averaged to derive $\mathbf{M}$ (λ), the mean noised profile for the chunk, and is given by

$$\mathbf{M}(\lambda)_i = \frac{1}{N_i} \sum_{q=1}^{N_i} L_T(\lambda)_{i,\,\mathbf{p}(q)}. \tag{5}$$

An estimate of the true mean profile of the chunk is derived by smoothing $\mathbf{M}(\lambda)$ with a running mean of length L to derive the mean vector, $\mathbf{R}(\lambda)$ for the ith detector is

given by

$$R(\lambda)_i = \frac{1}{N'} \sum_{l=i-L/2}^{i+L/2} \mathbf{M}(\lambda)_l \tag{6}$$

The image edge effects are minimised by averaging only the number of remaining pixels to the right and left of the central pixel, and N' is the number of detectors with pixels over water between i-$L/2$ and $i+L/2$. The length of the running mean is configurable in the software implementation of the ADM; however, a default value of 30 detectors is used for images shown in this paper. Figure 3 shows an example of the derived vector $\mathbf{M}(\lambda)$ and the resulting vector $\mathbf{R}(\lambda)$ for a subsection of a chunk.

After deriving $\mathbf{M}(\lambda)_{i,k}$ and $\mathbf{R}(\lambda)_{i,k}$ for each kth chunk, a matrix of correction coefficients, $\mathbf{C}(\lambda)$, is derived using

$$\mathbf{C}(\lambda)_{i,k} = \frac{R(\lambda)_{i,k}}{M(\lambda)_{i,k}} \tag{7}$$

The correction coefficient that will be applied to all pixels in the image from the ith detector is derived from the $\mathbf{C}(\lambda)_{i,k}$ from all k chunks. The closest $\mathbf{C}(\lambda)_{i,k}$ are averaged together and outliers are ignored using an exclusion function, $f_{\text{exclusion}}$ which only includes $\mathbf{C}(\lambda)_{i,k}$ that are not equal to 1.0 and are greater than 0.8 and less than 1.2,

$$K(\lambda)_i = \frac{1}{N''} \sum_{k=1}^{h} f_{\text{exclusion}}\left(\mathbf{C}(\lambda)_{i,k}\right) \tag{8}$$

where h is the total number of chunks used from the image and N'' is the total number of included $\mathbf{C}(\lambda)_{i,k}$. Care is taken to ensure that when image subset processing is conducted, at least three chunks are available to use in the ADM for

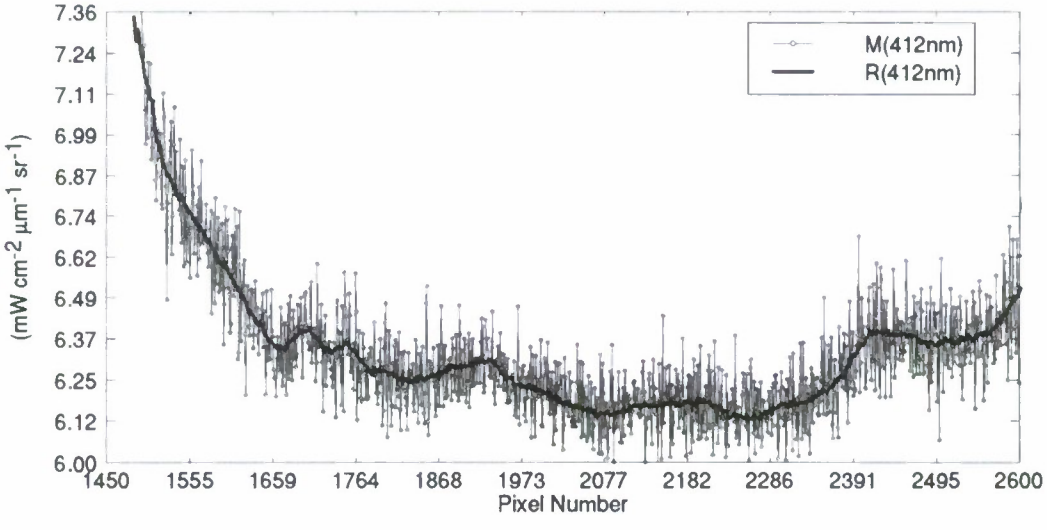

Figure 3. A subsection plot of the mean radiance of an image chunk, **M**(412 nm) along with the smoothed running mean, **R**(412 nm), which is an estimate of the true mean radiance of the image chunk.

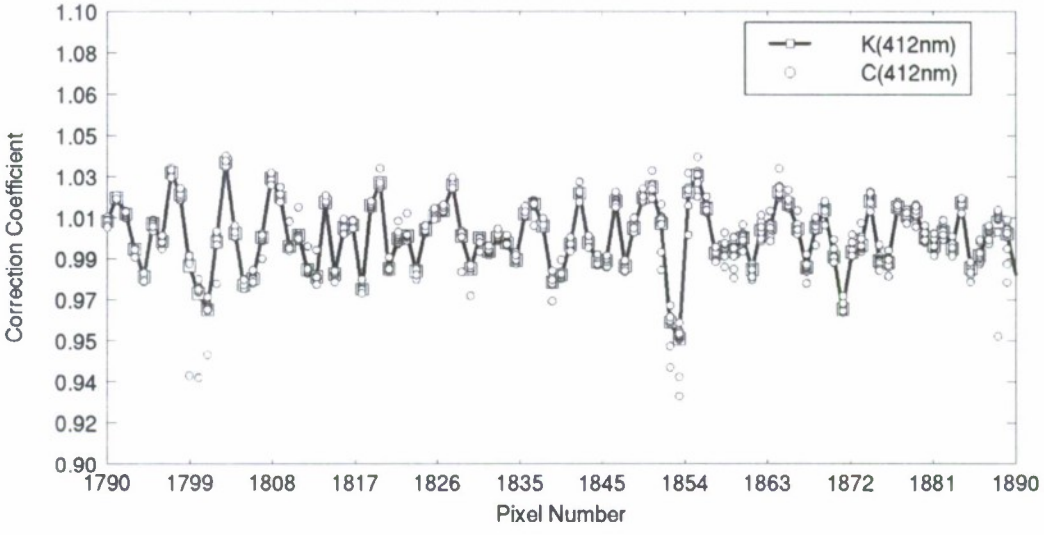

Figure 4. A subsection plot of the correction coefficients, **C**(412 nm), for each kth chunk along with the final correction coefficient, **K**(412 nm) derived from the mean of the un-excluded values of **C**(412 nm).

the exclusion function described above to work properly. The derived correction coefficient vector, $\mathbf{K}(\lambda)$, is used to correct the entire image. This process is repeated for all spectral channels. The atmospheric correction and in-water optical properties algorithms are applied to the de-striped spectral channels. Figure 4 shows an example of a $\mathbf{C}(412\,\text{nm})_{i,k}$ and the resulting $\mathbf{K}(412\,\text{nm})_i$ for a subsection of all detectors.

3. Results

Figure 5 shows $L_T(412\,\text{nm})$ that has been de-striped with the ADM. Note that there is some residual striping left in the image. However, overall, the majority of the

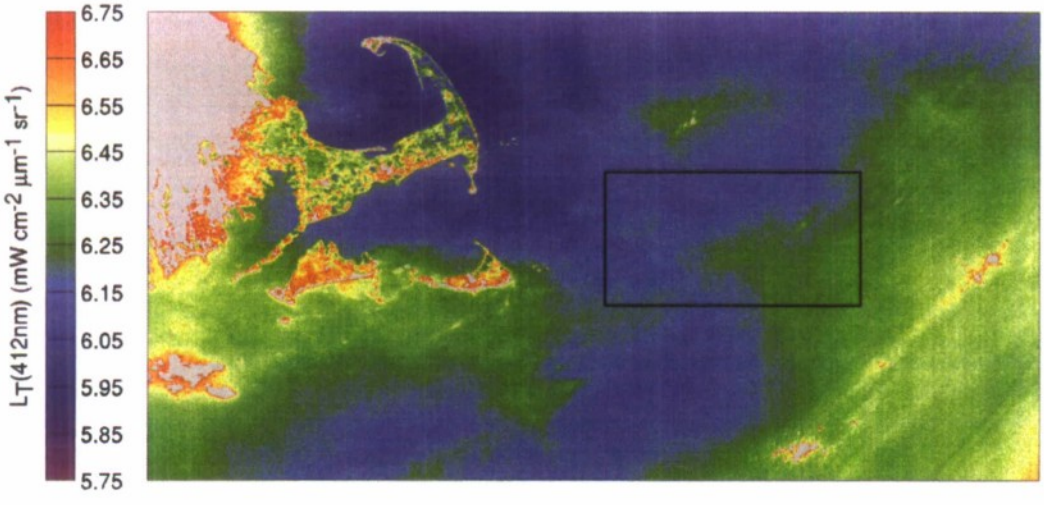

Figure 5. A false colour image of a subsection of OCM top of atmosphere radiance $L_T(412\,\text{nm})$, de-striped by the ADM. Note there is some residual striping remaining in the image, however the majority of the striping artifacts have been removed. The black square shows the sub-region of the data used in figure 7 below.

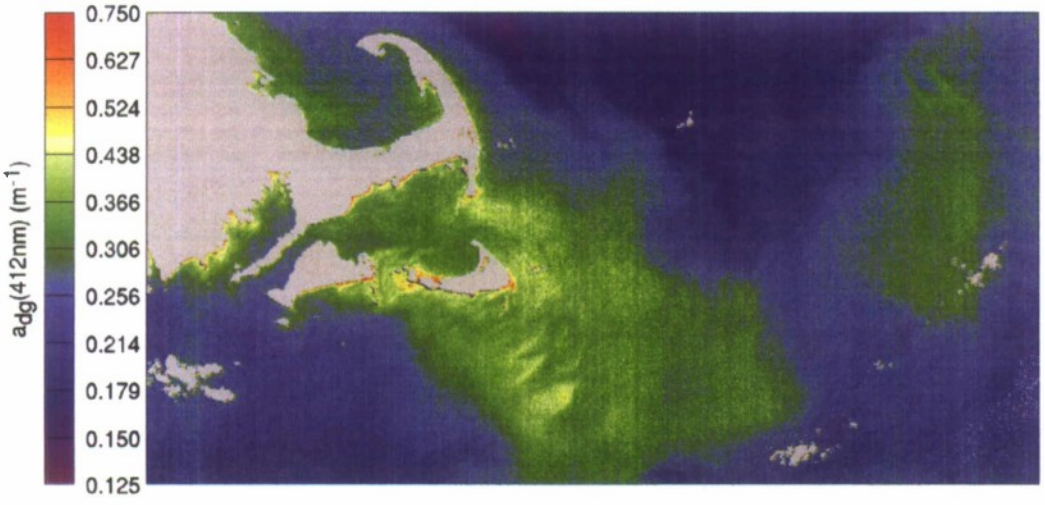

Figure 6. A false colour image of a subsection of coloured dissolved organic matter absorption coefficient at 412 nm, $a_{dg}(412\,nm)$ derived from ADM de-striped radiance. The in-water features can be discerned much more easily from this image than from the image of the same product derived from striped OCM data as shown in figure 2.

detector to detector variation has been removed. (The box inset is discussed in the section describing Figure 7 below.)

The ADM was then applied to all other spectral channels to remove striping from all top of atmosphere radiance channels. The resulting de-striped $L_T(\lambda)$ images were then passed through the atmospheric correction routines in MSl12 and the QAA to produce the dissolved organic matter absorption at 412 nm, $a_{dg}(412\,nm)$, image shown in Figure 6. The QAA uses at least five bands, including the atmospheric correction process. All the residual striping that is remaining in all the radiance images (not shown) used in QAA and atmospheric correction impact the derived

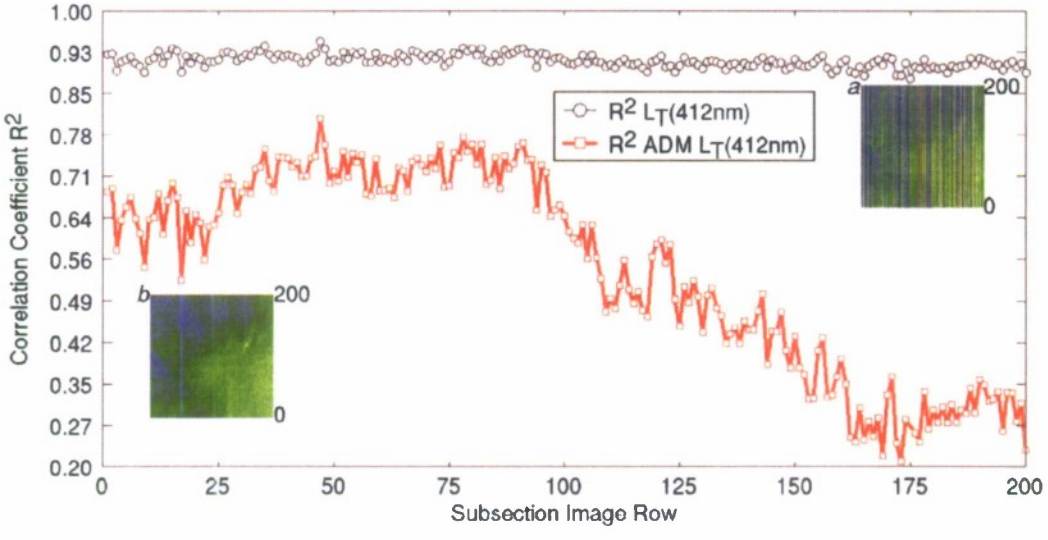

Figure 7. Inter-line correlations of a striped and an ADM de-striped 201 × 201 pixel sub-region of top of atmosphere radiance at 412 nm, $L_T(412\,nm)$. The level of inter-line correlation of the striped sub-region is driven by the striping, where the level of inter-line correlation of the de-striped sub-region is driven by the spatial variability of $L_T(412\,nm)$.

products, therefore there is more residual striping in the a_{dg}(412nm) image than found in any individual $L_T(\lambda)$.

To quantify the efficiency of the ADM, the correlation of each scan line to the next scan line is calculated for a subsection of L_T as described by the box shown in figure 5. Figure 7 shows the correlation coefficients for both striped and de-striped image subsections for the 200 rows used. Inset image (a) is the striped L_T(412 nm) and the inset image (b) is the ADM de-striped L_T(412 nm). The degree of striping induced correlation in the striped L_T(412 nm) subsection is quite high, having a mean R^2 value of 0.911. The subsection from the ADM processed image has a much lower mean R^2 value of 0.547 and is variable across image, as would be expected for a scene over water.

Figure 8 shows the histograms of L_T(412 nm) shown in the striped image in figure 1 and the de-striped image shown in figure 5. The distribution of the de-striped values has a pronounced peak in the distribution at 6.14 mW cm^{-2} μm^{-1} sr^{-1} where the striped image peak distribution is located at 6.21 mW cm^{-2} μm^{-1} sr^{-1}. However, the mean values of both the striped and de-striped images remain the same at 6.34 mW cm^{-2} μm^{-1} sr^{-1}.

4. Discussion

The ADM de-striping algorithm described here does not require a homogenous water mass to derive the correction coefficient for each detector. As stated above, the ADM does require that the errors in detector characterization have higher spatial variability than the spatial variability of the in-water features. The ADM will fail to derive correction coefficients where the spatial variability of *all* image chunks is on the order of the variability of the errors in the detector characterization. Also,

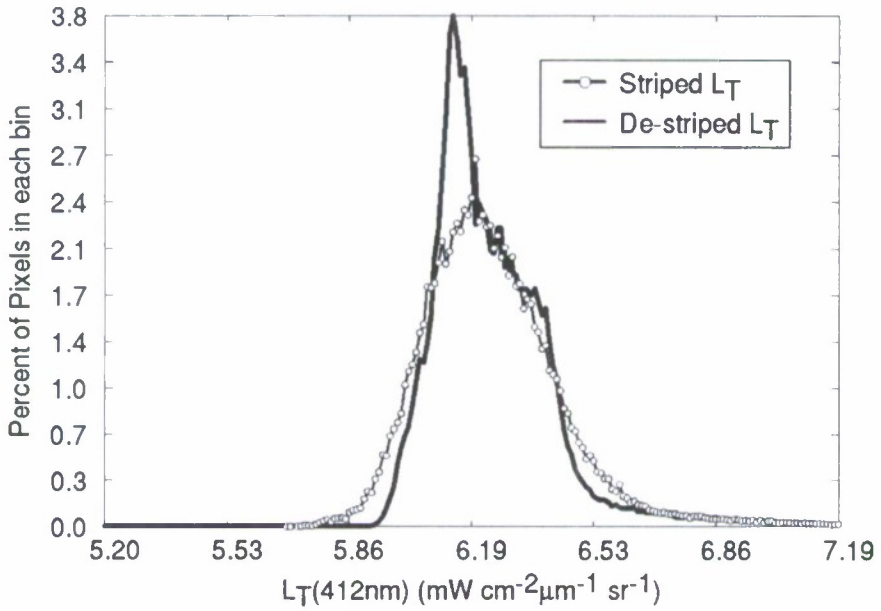

Figure 8. Histograms of the section of data shown in figure 1 (striped L_T(412 nm)) and figure 5 (de-striped L_T(412 nm)). The mean value for both image sections remains the same, 6.34 mW cm^{-2} μm^{-1} sr^{-1}, however peak of the de-striped distribution is located at 6.14 mW cm^{-2} μm^{-1} sr^{-1} verses 6.21 mW cm^{-2} μm^{-1} sr^{-1} for the striped image distribution.

in order to derive a correction coefficient for a particular detector, there needs to be several sections of contiguous data in the image from the detector that contain radiances measured over water. Therefore, the ADM will not be able to derive correction coefficients for portions of some images owing to the distributions of clouds or land.

Products derived from the ADM de-striped top of atmosphere OCM images show vast improvement over the raw OCM top of atmosphere radiances and products derived from those radiances. Without a de-striping algorithm applied, most imagery derived from OCM would not be usable for most purposes. There are many other published image de-striping techniques that are used to de-stripe other satellite data. However, de-striping techniques that rely on a fixed sensor state are not applicable to OCM data owing to the procedures used to operate the satellite, where the sensor is turned on only for purchased passes. Also the de-striping techniques that remove frequencies associated with the periodicity of the striping caused by multiple along track detectors per band which are scanned across a scene, will not work on OCM data because OCM is a push-broom design.

The ADM described here could be modified to work with other sensors with a push-broom design. The key parameters that control the performance of the ADM, such as the chunk size, and the running mean length, L, would need to be optimised for another sensor if the spatial resolution of the other sensor is not similar to the spatial resolution of OCM. It is also important that the errors in the characterization of the detectors of the sensor have higher variability than the natural spatial variability of the in-water features.

Further study will be conducted to perform a vicarious calibration using de-striped OCM data. A vicarious calibration will improve the quality of products derived from the OCM de-striped data (Eplee *et al.* 2001). This refinement calibration could not be conducted on striped OCM data.

References

AHERN, F.J., BROWN, R.J., CIHLAR, J., GAUTHIER, R., MURPHY, J., NEVILLE, R.A. and TEILLET, P.M., 1984, Radiometric correction of visible and infrared remote sensing data at the Canada Center for Remote Sensing. *International Journal of Remote Sensing*, **8**, pp. 1349–1376.

CHEN, J., LIN, H., SHAO, Y. and YANG, L., 2006, Oblique striping removal in remote sensing imagery based on wavelet transform. *International Journal of Remote Sensing*, **27**, pp. 1717–1723.

CHEN, J., SHAO, Y., GUO, H., WANG, W. and ZHU, B., 2003, Destriping CMODIS data by power filtering. *IEEE Transactions on Geoscience and Remote Sensing*, **41**, pp. 2119–2124.

CORSINI, G., DIANI, M. and WALZEL, T., 2000, Striping removal in MOS-B data. *IEEE Transactions on Geoscience and Remote Sensing*, **38**, pp. 1439–1446.

CRIPPEN, R.E., 1989, A simple spatial filtering routine for the cosmetic removal of scan-line noise from Landsat TM P-tape imagery. *Photogrammetric Engineering and Remote Sensing*, **55**, pp. 327–331.

EPLEE, R.E., ROBINSON, W.D., BAILEY, S.W., CLARK, D.K., WERDELL, P.J., WANG, M., BARNES, R.A. and MCCLAIN, C.R., 2001, Calibration of SeaWiFS. II. Vicarious techniques. *Applied Optics*, **40**, pp. 6701–6718.

FISCHEL, D., 1984, Validation of the Thematic Mapper radiometric and geometric correction algorithms. *IEEE Transactions on Geoscience and Remote Sensing*, **22**, pp. 237–242.

GADALLAH, F.L., CSILLAG, F. and SMITH, E.J.M., 2000, Destriping multisensor imagery with moment matching. *International Journal of Remote Sensing*, **21**, pp. 2505–2511.

HORN, B.K.P. and WOODHAM, R.J., 1979, Destriping Landsat MSS images by histogram modification. *Computer Graphics and Image Processing*, **10**, pp. 69–83.

LEE, Z., CARDER, K.L. and ARNONE, R.A., 2002, Deriving inherent optical properties from water colour:a multiband quasi-analytical algorithm for optically deep waters. *Applied Optics*, **41**, pp. 5755–5772.

POROS, D.J. and PETERSON, C.J., 1985, Methods for destriping Landsat Thematic Mapper images: A feasibility study for an online destriping process in the Thematic Mapper Image Processing System (TIPS). *Photogrammetric Engineering and Remote Sensing*, **51**, pp. 1371–1378.

SIMPSON, J.J., STITT, J.R. and LEATH, D.M., 1998, Improved finite impulse response filters fro enhanced destriping of geostationary satellite data. *Remote Sensing of the Environment*, **66**, pp. 235–249.

WEGENER, M., 1990, Destriping multiple sensor imagery by improved histogram matching. *International Journal of Remote Sensing*, **11**, pp. 859–875.